Published in final edited form as:
Acta Biomater. 2011 June ; 7(6): 2394–2400. doi:10.1016/j.actbio.2011.02.032.

Silk Fibroin Electrogelation Mechanisms

Qiang Lu[a,b,c,*], **Yongli Huang**[a], **Mingzhong Li**[a], **Baoqi Zuo**[a], **Shenzhou Lu**[a], **Jiannan Wang**[a], **Hesun Zhu**[d], and **David L. Kaplan**[c]

[a]National Engineering Laboratory for Modern Silk, College of Textile and Clothing Engineering, Soochow University, Suzhou 215123, People's Republic of China

[b]Jiangsu Province Key Laboratory of Stem Cell Research, Soochow University, Suzhou 215006, People's Republic of China

[c]Department of Biomedical Engineering, Tufts University, Medford, MA 02155, USA

[d]Research Center of Materials Science, Beijing Institute of Technology, Beijing, 100081, People's Republic of China

Abstract

A silk fibroin gel system (e-gel), formed with weak electric fields has potential utility in medical materials and devices. The mechanism of silk e-gel formation was studied to gain additional insight into the process and control of the material properties. Silk fibroin nanoparticles with sizes of several ten nanometers, composed of metastable conformations, were involved in e-gel formation. Under electric fields, the nanoparticles rapidly assembled into larger nano- or microspheres with size ranges from tens nanometers to several microns. Repulsive forces from the negative surface charge of the acidic groups on the protein were screened by the local decrease in solution pH in the vicinity of the positive electrode. By controlling the formation and content of silk fibroin nanoparticles e-gel could be formed even from low concentration silk fibroin solutions (1%). When e-gel was reversed to the solution state, the aggregated nano- and microspheres dispersed into solution, a significant observation related to future applications for this process, such as for drug delivery.

Keywords

silk fibroin; electrogelation; nanoparticle; microspheres

1. Introduction

Silk fibroin from the cocoons of the silkworm *Bombyx mori* has recently been explored as a versatile protein biomaterial for the formation of films, fibers, microspheres and porous scaffolds for a number of applications bridging the biomedical and physical sciences [1–7]. For example, silk fibroin has been processed in aqueous solution to fabricate porous 3D tissue scaffolds [8], as well as biophotonic thin films [9]. The same solution can also be blended with other polymers and bioactive dopants and freeze-dried into microspheres [10]. The biocompatibility and biodegradability of the silk fibroin protein allow silk-based biomaterials to be used in vivo [11]. Furthermore, the functionality of silk fibroin can be increased by chemical modifications to acid or tyrosine side chains [12].

Corresponding author: Qiang Lu, National Engineering Laboratory for Modern Silk, College of Textile and Clothing Engineering, Soochow University, Suzhou 215021, People's Republic of China, TeL: (+86)-512-67061649; Lvqiang78@suda.edu.cn.

Silk hydrogels have been studied for biotechnological applications. The hydrogelation of silk fibroin is triggered in aqueous solution with conditions such as low pH, high temperature or high ionic strength [13], or alternatively in physiologically relevant solution conditions via ultra sonication or with vortexing as energy inputs [14, 15]. In these silk hydrogel systems, the formation of hydrated networks was due to an increase of non-covalent, but essentially irreversible, intra- and intermolecular β-sheet crosslinks. Recently, we reported an electrically mediated hydogel (e-gel) from silk fibroin [16, 17]. The e-gel system, mainly composed of random structure rather than β-sheet, involved a temperature reversible, dynamic self-assembly of the silk protein. The interesting control of gel formation, the reversibility and the adhesion features of the silk e-gel suggest applications in medical, environmental, and device fields [16, 17]. However, the mechanisms involved in the e-gel systems remain to be fully defined. Such insight would further the control of the e-gel process as well as utility towards specific applications. Currently, the understanding of e-gel mechanisms is based on structural and mechanical results [17]. The increase in proton concentration in the vicinity of the positive electrode due to the applied electric field was a predominant factor in electrogelation. The local decrease in solution pH leads to screening of the acidic surface charged groups enabling intermolecular self-assembly events. However, the present mechanism is not complete and additional insight is needed in order to be able to better control electrogelation.

The goal of the present study was to provide additional insight into the mechanisms of the e-gel process. Toward this goal, changes in morphology and secondary structures before and after the gel formation were assessed to clarify pivotal factors that control electrogelation. Second, by adjusting these pivotal factors, e-gel formation was controlled to confirm this new mechanistic insight. Finally, the nanostructures associated with reversed silk e-gel solutions were investigated to gain additional insight into the overall process.

2. Experimental

2.1 Preparation of aqueous silk fibroin solutions

Silk fibroin aqueous solutions were prepared as previously described [18]. Briefly, *B. mori* cocoons were boiled for 20 min in an aqueous solution of 0.02 M sodium carbonate and then rinsed thoroughly with deionized water. After overnight drying, the silk fibroin was dissolved in an aqueous solution containing 9.3 M LiBr at 60°C. The solution was dialyzed against deionized water using Slide-a-Lyzer dialysis cassettes (Pierce, molecular weight cut-off 3,500) for 72 h to remove the salt. The solution was optically clear after dialysis and was centrifuged to remove small amounts of aggregates that formed during the process. The final concentration of aqueous silk fibroin solution was ~8 wt%, determined by weighing the remaining solid after drying. The fresh silk fibroin solution was stored at 4°C at least 2 weeks for aging. Only the aged silk fibroin solution formed e-gel under the electric field.

2.2 Electrogelation of silk fibroin solutions

Using our previously described process, electrodes were immersed in an aqueous solution of silk fibroin and 25 V_{DC} was applied over a 3 minute period to a pair of conductive electrodes [16]. Within seconds of the application of the voltage, a visible gel formed at the positive electrode.

2.3 Silk fibroin solution treatments

To assess mechanisms of electrogelation, the nanostructure of silk fibroin in aqueous solution was controlled in different ways. First, the fresh silk fibroin solution (~8 wt%) was incubated for 24 hr at 60°C to assemble into nanoparticles that remained stable in aqueous solution, and then diluted from 8 wt% to 4 wt%, 2 wt% and 1 wt%, respectively. Second, the

fresh silk solution was slowly concentrated at 60°C by controlling drying. After 72 hr, the concentration of the silk fibroin increased to about 30 wt%. This concentrated silk fibroin solution was then diluted to 8 wt%, 4 wt%, 2 wt% and 1 wt%, respectively. In contrast to the silk fibroin solution incubated at 60°C, the concentrated silk fibroin solution mainly consisted of nanofilaments. Subsequently, the electrodes were immersed in the above treated solutions and 25 V_{DC} was applied over a 3 minute period to induce the gelation process.

2.4 Reversion from e-gel to solution

The e-gel was first extracted several times with distilled water to remove any free (ungelled) silk fibroin. The extracted e-gel was placed in cellulose dialysis tubes (MWCO 3,500) and then placed in an aged silk fibroin solution (8 wt%). The electrical process was reversed, as shown previously [16, 17], by immersing the negative electrode in the e-gel inside the cellulose tube with the positive electrode in the aged silk fibroin solution outside the tube, respectively, and treating the system fro 3 minutes at 25 V. The morphology of the silk fibroin in the reversed solution inside the cellulose tube was investigated by SEM and particle size analysis.

2.5 Fourier Transform Infrared Spectroscopy (FTIR)

The structural changes in the silk solution and gel states were analyzed using a JASCO FTIR 6200 spectrometer (JASCO, Tokyo, Japan) equipped with a MIRacle™ attenuated total reflection (ATR) Ge crystal cell in reflection mode. For FTIR experiments, all samples were flash frozen and dried in liquid nitrogen to preserve the original structure as accurately as possible. Control experiments conducted on hydrated samples, produced data similar to that collected from freeze-dried samples. Background measurements were taken with an empty cell for freeze-dried samples or from deionized water in the case of hydrated samples and the data were subtracted from the sample readings. For each measurement, 32 scans were coded with a resolution of 4 cm^{-1}, with the wavenumber ranging from 400–4000 cm^{-1}. Fourier self-deconvolution (FSD) of the infrared spectra covering the amide I region (1595–1705 cm^{-1}) was performed by Opus 5.0 software to identify silk secondary structures. Deconvolution was performed using Lorentzian line shape with a half-bandwidth of 25 cm^{-1} and a noise reduction factor of 0.3. FSD spectra were curve-fitted to measure the relative areas of the amide I region components [19].

2.6 Differential Scanning Calorimetry (DSC)

The lyophilized samples were encapsulated in aluminum pans and heated in a TA Instruments Q100 DSC (TA Instruments, New Castle, DE) with a dry nitrogen gas flow of 50 ml/min. The instrument was calibrated for empty cell baseline and with respect to an indium standard for heat flow and temperature. The samples were heated at 2°C/min from −30°C to 350°C with a modulation period of 60 s and temperature amplitudes of 0.318°C.

2.7 Scanning Electron Microscopy (SEM)

The e-gel samples were extracted several times with distilled water to remove any adhered silk solution. Then the lyophilized samples were platinum-coated and examined morphologically by Scanning Electron Microscopy (SEM, Supra 55 VP, Zeiss, Oberkochen, Germany).

2.8 Atomic force microscopy (AFM)

The morphology of silk fibroin in solution and in the e-gel were observed by AFM (Veeco, Nanoscope III) in air. A 225 μm long silicon cantilever with a spring constant of 3 N/m was used in tapping mode. In order to remove the effect of silk solution, the e-gel was extracted several times with distilled water before characterization.

2.9. Measurement of particle sizes

The changes in silk morphology in the reversed solution were analyzed by Particle size analyzer (Malvern, Mastersizer 2000, Worcestershire, United Kingdom) in a solution at 25°C. According to the analyzer procedure, the silk fibroin solution was diluted to 2.5×10^{-3} % (w/v) and measured without filtering.

3. Results and discussion

3.1 Structural changes in the electrogelation process

In our previous studies e-gel was difficult to form if the silk solution was freshly prepared or when the silk fibroin concentrations were relatively low, for example below 7 wt%. Structural changes after the storage and subsequent electrogelation of silk solutions were therefore evaluated by FTIR and DSC (Figs. 1A and 1B). The FTIR spectral region between 1600 and 1700 cm^{-1} is commonly assigned to the absorption of the peptide backbone in secondary structures of silk fibroin. FTIR data collected from lyophilized samples of freshly prepared silk fibroin solution (8 wt%), aged (stored 2 weeks at 4°C) silk fibroin solution and e-gel indicated that the amide I peak shifted slightly from 1640 to 1650 cm^{-1} due to storage and then to 1660 cm^{-1} after e-gel formation, with no peak or shoulder between 1610 and 1630 cm^{-1} that could be attributed to specific β-sheet absorption. Deconvolution of these spectra demonstrated a statistically significant increase in turns, a decrease in random coil content, and no change in beta sheet content when comparing the fresh silk fibroin solution (8 wt%) to the aged solution (Table 1). The e-gel formation resulted in a further decrease in random coil content and a significant increase of α-helix. These results suggested intermediate conformations rather than β-sheet formation in silk e-gel. Importantly, these results indicated that the transformation from random coil to intermediate structures might be critical for the electrogelation.

In the heating process with DSC, the fresh silk solution did not show any crystallization peaks, indicating that the amorphous structures of silk in the fresh solution did not rearrange to form crystal structures. The other samples, including aged silk fibroin solution and the e-gel, showed a nonisothermal crystallization peak between 200 and 215°C, indicating that the structure was mainly amorphous. The amorphous silk transformed to β-sheets above the glass-transition temperature, T_g. Interestingly, the crystallization peak appeared at 213°C after storage for 2 weeks and, then further decreased to 206°C after e-gel formation, suggesting that intermediate, metastable conformations formed in the storage process, which further changed after electrogelation. The results also suggested the importance of the formation of intermediate structures for electrogelation, in good agreement with the FTIR data.

3.2 Nanostructural changes in the electrogelation process

The morphological features of the e-gel were assessed by SEM and AFM (Fig 2a,b). The microscopy images collected from e-gel samples were lyophilized at −80°C and exhibited spherical, micelle, micrometer-scale structures, with the size range from several tens of nanometers to several microns. Interestingly, the larger microspheres with diameter of microns were assembled from the small microspheres with diameters of several hundred or several tens of nanometers. In addition, these small microspheres were composed of smaller particles with diameters of about ten nanometers (Fig 2c,d). The results suggested that e-gel was assembled from nanoparticles with sizes of about ten nanometers under electric fields. The hierarchical structure of silk fibroin microspheres was compatible with the aggregate structures of silk fibroin in many other studies. In our previous study, a model of silk formation in insects emphasized the formation and then aggregation of micelles with sizes of 100–200 nm diameter [20, 21]. The micelles formed in silk/PEO have similar sizes with the

microspheres formed under electric fields. Recently, new silk aggregation mechanisms indicate that the aggregates (d_{max}=260 nm) were composed of silk fibroin with sizes of 16 nm diameter [22]. More recently, silk fibroin micelles with silk I structure were assembled by slow drying to mimic the natural silk processing. The micelles assembled by slow drying were composed of nanofilaments that consisted of nanoparticles with size of 10–80 nm diameter [23, 24]. Based on these studies, silk fibroin nanoparticles with sizes of several ten nanometers appear to be a basic assembly component.

The nanostructure of silk fibroin in fresh and aged solutions was investigated. Interestingly, silk fibroin in the fresh solution mainly maintained random coil structure without specific nanostructures, and then assembled to nanoparticles after the storage for 2 weeks at 4°C (Fig. 3). Based on the conformation and nanostructure results, these nanoparticles with sizes of tens of nanometers composed of intermediate turns, were an important precondition for the e-gel formation process under electric fields.

In neutral aqueous solution, the overall negative surface charge due to the acidic charged groups prevent intermolecular self-assembly. In the electric field, the proton concentration increases in the vicinity of the positive electrode, resulting in the local decrease in solution pH and the screening of the acidic surface charged groups, allowing silk fibroin to assemble [17]. When silk fibroin maintained a random coil structure, extensive time and energy were required to rearrange the hydrophobic and hydrophilic domains in the silk fibroin chains, so intermolecular self-assembly for gelation, did not occur during the relatively short time in electric fields. Once the hydrophobic and hydrophilic domains of the protein chains had rearranged and assembled into nanoparticles, the negative charge was possibly a predominant factor to prevent intermolecular self-assembly. Therefore, the nanoparticles aggregated quickly to form e-gel under the applied electric fields because of screening of the charged groups (Fig 4). At the same time, the hydrophobic and hydrophilic domains further assembled to form more regular and compact structures (Fig. 1), resulting in nanoparticles reducing in size from tens of nanometers to about ten nanometers (Fig 2).

3.3 Validation of electrogelation mechanism

In order to confirm these observations, silk solutions with different nanostructures were prepared. Silk fibroin was mainly composed of random coil structures in fresh solution (Fig 5a), and then assembled into nanoparticles after aging for 8 hr at 60°C (Fig 5b). The fresh silk solution was also concentrated slowly at 60°C for 3 days to generate concentrated solution (30 wt%). In the concentrated solution, silk fibroin further assembled from nanoparticles to nanofilaments (Fig 5c). The different solutions were diluted to 8 wt%, 4 wt %, 2 wt% and 1 wt%, respectively, and treated under same electric field as used above. When silk fibroin was mainly composed of nanoparticles after aging at 60°C, electrogelation occurred even at low concentrations (4 wt%, 2 wt% and 1 wt%). Electrogelation was quicker and easier if the formation of nanoparticles preceded the process. After nanoparticles further assembled into nanofilaments, electrogelation did not occur even at high silk fibroin concentration (8 wt%) (Fig 6 and Table 2). These results confirmed that nanoparticles were a critical precondition for e-gel formation. By controlling the formation of nanoparticles in silk fibroin solution, it was possible to control electrogelation.

3.4 Reversibility of silk fibroin electrogelation

In our previous studies, the e-gel system was a reversible material system [16]. The reversibility was controlled by the reversal of the electric field or with a slight increase in temperature. In present study, the e-gel was placed in a cellulose tube to keep from blending with silk fibroin solution in reversing process. As shown in Fig. 7, the nano- or microspheres were retained in the reversed solution. The nano- or microspheres only dispersed into the

solution rather than separated into smaller particles. Under the electric field, the nanoparticles aggregated into compact nano- or microspheres (Fig 2) that were stable through a reversal of the electrical process. FTIR and DSC results confirmed the formation of more compact and stable structures. The micromorphology of the e-gel (Fig 2) also showed that there was little connection among the nano- or microspheres. Once the electrodes were reversed, the negative charge reappeared among the nano- or microspheres, dispersing them into solution. The processing conditions had a significant influence on the stability of the e-gel. Following the increase of electrogelation time and silk fibroin concentrations, the e-gel achieved higher stability and was more difficult to return to the solution state, since stronger interactions formed between among the nano- and microspheres.

4. Conclusions

Studies aimed at the mechanism of silk electrogelation were conducted. The self-assembly of silk fibroin from random coil to metastable nanoparticles, with sizes of tens of nanometers was found as a critical step for the formation of e-gel. In electric fields, the nanoparticles aggregated to form nano- or microspheres with size ranges from tens of nanometers to several microns on the positive electrodes because of screening of the negative surface charge that could otherwise prevent intermolecular self-assembly of silk fibroin in neutral solution. The nano- or microspheres were still stable upon reversing the process, implying a novel way to prepare silk release systems in the future.

Acknowledgments

We thank the AFOSR, the NSF and National Natural Science Foundation of China (30970714) for support of this work.

References

1. Vepari C, Kaplan DL. Silk as a biomaterial. Prog Polym Sci. 2007; 32:991–1007. [PubMed: 19543442]
2. Wang XQ, Wenk E, Matsumoto A, Meinel L, Li CM, Kaplan DL. Silk microspheres for encapsulation and controlled release. J Control Release. 2007; 117:360–370. [PubMed: 17218036]
3. Karageorgiou V, Tomkins M, Fajardo R, Meinel L, Snyder B, Wade K, et al. Porous silk fibroin 3-D scaffolds for delivery of bone morphologenetic protein-2 in vitro and in vivo. J Biomed Mater Res A,. 2006; 78A:324–334. [PubMed: 16637042]
4. Wang M, Jin HJ, Kaplan DL, Rutledge GC. Mechanical properties of electrospun silk fibers. Macromolecules. 2004; 37:6856–6864.
5. Jin HJ, Park J, Vallzzi R, Cebe P, Kaplan DL. Biomaterial films of *Bombyx Mori* silk fibroin with poly (ethylene oxide). Biomacromolecules. 2004; 5:711–717. [PubMed: 15132651]
6. Jiang CY, Wang XY, Gunawidjaja R, Lin YH, Gupta MK, Kaplan DL, et al. Mechanical properties of robust ultrathin silk fibroin films. Adv Funct Mater. 2007; 17:2229–2237.
7. Liu HF, Fan HB, Wang Y, Toh SL, Goh JCH. The interaction between a combined knitted silk scaffold and microporous silk sponge with human mesenchymal stem cells for ligament tissue engineering. Biomaterials. 2008; 29:662–674. [PubMed: 17997479]
8. Li C, Vepari C, Jin HJ, Kim HJ, Kaplan DL. Electrospun silk-BMP-2 scaffolds for bone tissue engineering. Biomaterials. 2006; 27:3115–3124. [PubMed: 16458961]
9. Amsden JJ, Domachuk P, Gopinath A, White RD, Negro LD, Kaplan DL, et al. Rapid nanoimprinting of silk fibroin films for biophotonic applications. Adv Mater. 2010; 22:1746–1749. [PubMed: 20496408]
10. Wang XQ, Yucel T, Lu Q, Hu X, Kaplan DL. Silk nanospheres and microspheres from silk/pva blend films for drug delivery. Biomaterials. 2010; 31:1025–1035. [PubMed: 19945157]

11. Altman GH, Diaz F, Jakuba C, Calabro T, Horan RL, Chen J, et al. Silk-based biomaterials. Biomaterials. 2003; 24:401–416. [PubMed: 12423595]
12. Murphy A, John P, Kaplan DL. Modification of silk fibroin using diazonium coupling chemistry and the effects on hMSC proliferation and differentiation. Biomaterials. 2008; 29:2829–2838. [PubMed: 18417206]
13. Kim UJ, Park J, Li C, Jin HJ, Valluzzi R, Kaplan DL. Structure and properties of silk hydrogels. Biomacromolecules. 2004; 5:786–792. [PubMed: 15132662]
14. Wang XQ, Kluge JA, Leisk GG, Kaplan DL. Sonication-induced gelation of silk fibroin for cell encapsulation. Biomaterials. 2008; 29:1054–1064. [PubMed: 18031805]
15. Yucel T, Cebe P, Kaplan DL. Vortex-induced injectable silk fibroin hydrogels. Biophysical Journal. 2009; 97:2044–2050. [PubMed: 19804736]
16. Leisk GG, Lo TJ, Yucel T, Lu Q, Kaplan DL. Electrogelation for protein adhesives. Adv Mater. 2010; 22:711–715. [PubMed: 20217775]
17. Yucel T, Kojic N, Leisk GG, LO TJ, Kaplan DL. Non-equilibrium silk fibroin adhesives. J Struct Biol. 2010; 170:406–412. [PubMed: 20026216]
18. Kim UJ, Park J, Kim HJ, Wada M, Kaplan DL. Three-dimensional aqueous-derived biomaterial scaffolds from silk fibroin. Biomaterials. 2005; 26:2775–2785. [PubMed: 15585282]
19. Hu X, Kaplan DL, Cebe P. Determining Beta-sheet crystallinity in fibrous proteins by thermal analysis and infrared spectroscopy. Macromolecules. 2006; 39:6161–6170.
20. Rammensee S, Slotta U, Scheibel T, Bausch A. Assembly mechanism of recombinant spider silk proteins. PNAS. 2008; 105:6590–6595. [PubMed: 18445655]
21. Jin HJ, Kaplan DL. Mechanism of silk processing in insects and spiders. Nature. 2003; 424:1057–1061. [PubMed: 12944968]
22. Martel A, Burghammer M, Davies RJ, Cola ED, Vendrely C, Riekel C. Silk fiber assembly studies by synchrotron radiation SAXS/WAXS and Raman spectroscopy. JACS. 2008; 130:17070–17074.
23. Lu Q, Hu X, Wang XQ, Kluge JA, Lu SZ, Cebe P, et al. Water-insoluble silk films with silk I structure. ACTA Biomaterialia. 2010; 6:1380–1387. [PubMed: 19874919]
24. Lu Q, Wang XL, Lu SZ, Li MZ, Kaplan DL, Zhu HS. Nanofibrous architecture of silk fibroin scaffolds prepared with a mild self-assembly process. Biomaterials. 2010 (in press).

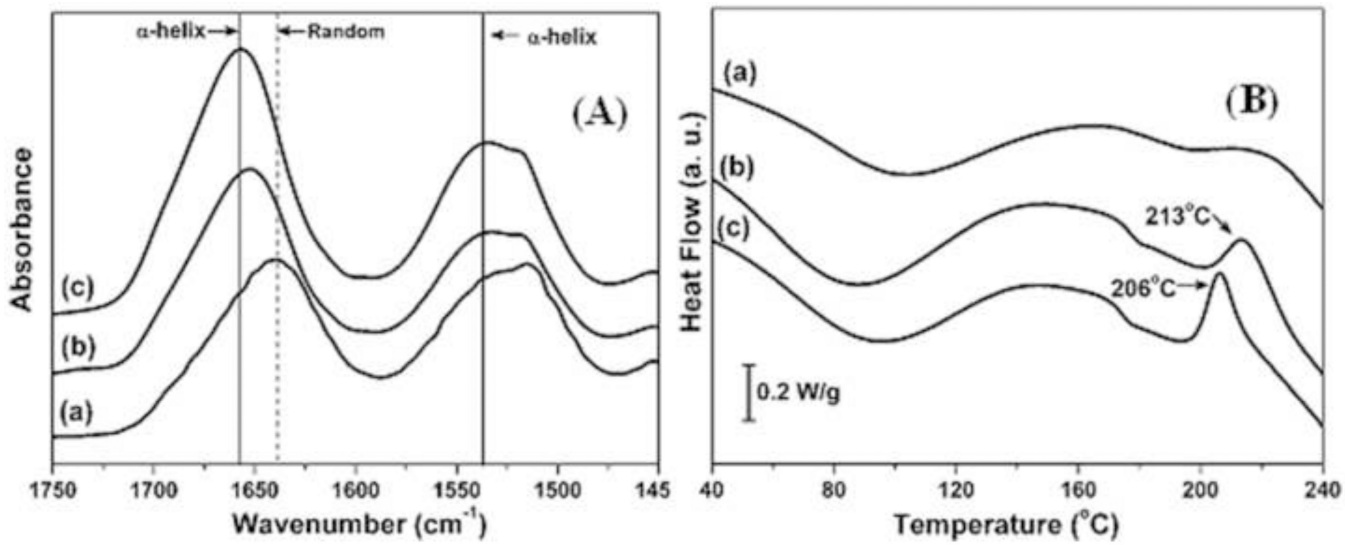

Figure 1.

A) FTIR data collected from lyophilized samples. (a) Fresh silk fibroin solution (8 wt%); (b) aged fibroin solution (8 wt%), (a) stored at 4°C for 2 weeks; (c) e-gel derived from (b). B) DSC scans collected from lyophilized samples prepared the same way as in (A).

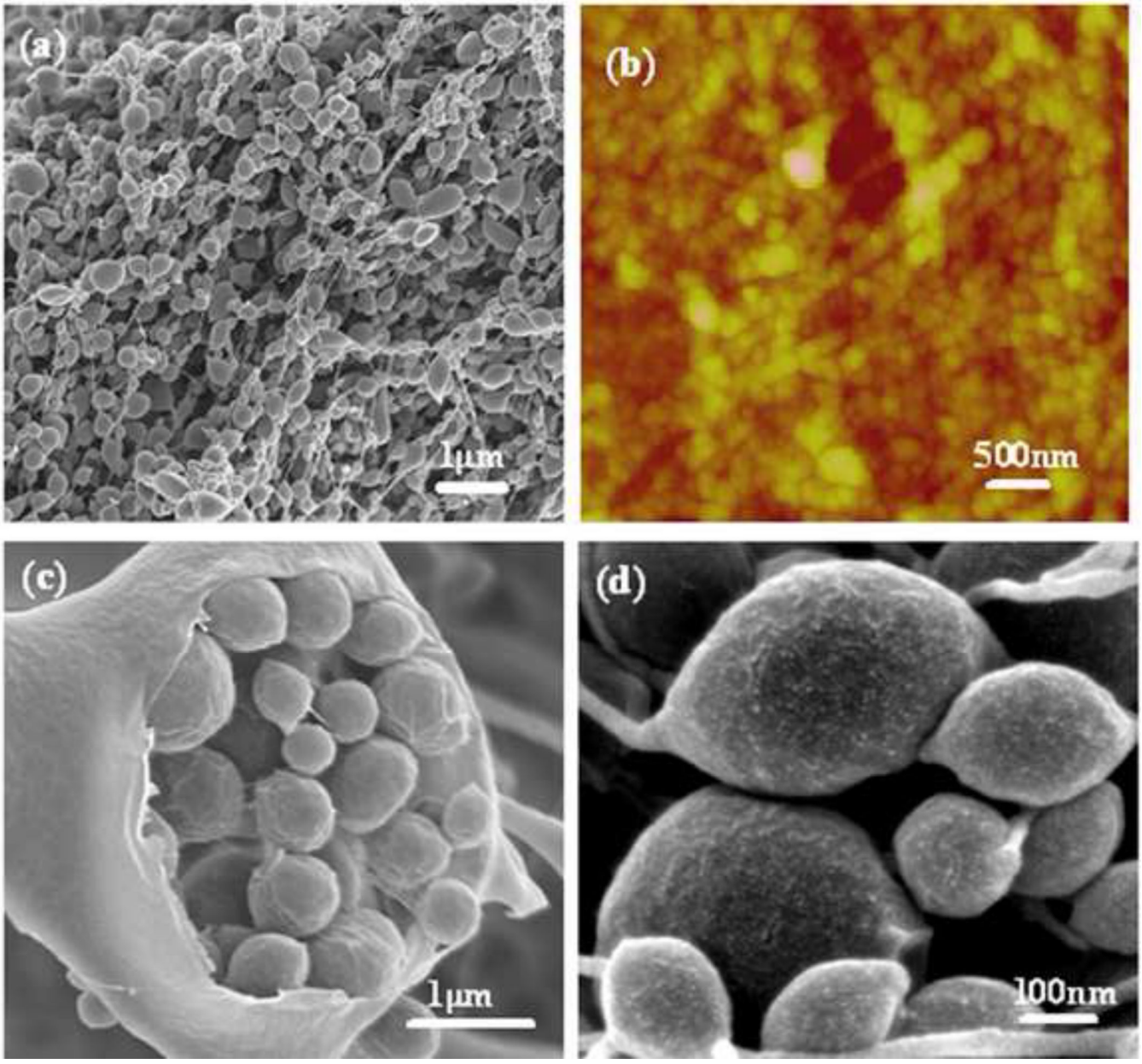

Figure 2.
Morphology of e-gel derived from 8wt% silk fibroin solution with 25 V_{DC} using mechanical pencil-lead electrodes: (a) SEM; (b) AFM; (c) inside structure of large microspheres in the e-gel; (d) magnified images of microspheres in the e-gel. The e-gel samples were extracted several times with distilled water to remove the adhered silk solution.

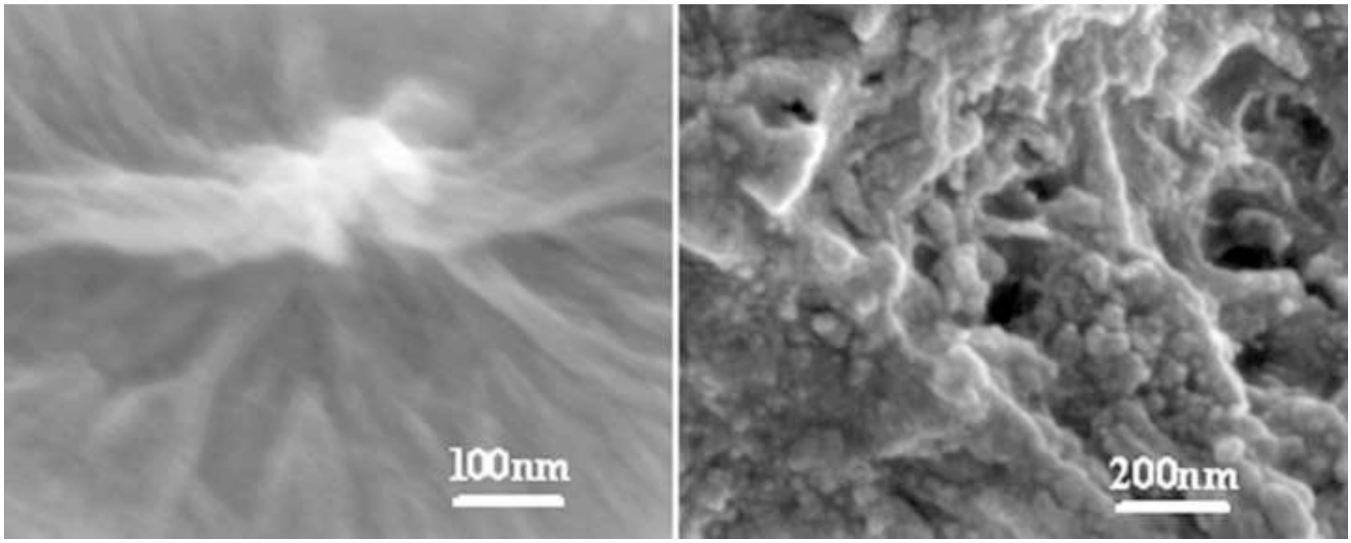

Figure 3.
SEM data from lyophilized samples: (a) fresh silk solution (8 wt%) and (b) aged silk fibroin solution (8 wt%), (a) stored at 4°C for 2 weeks. Nanoparticles tens of nanometers assembled in the aged silk solution.

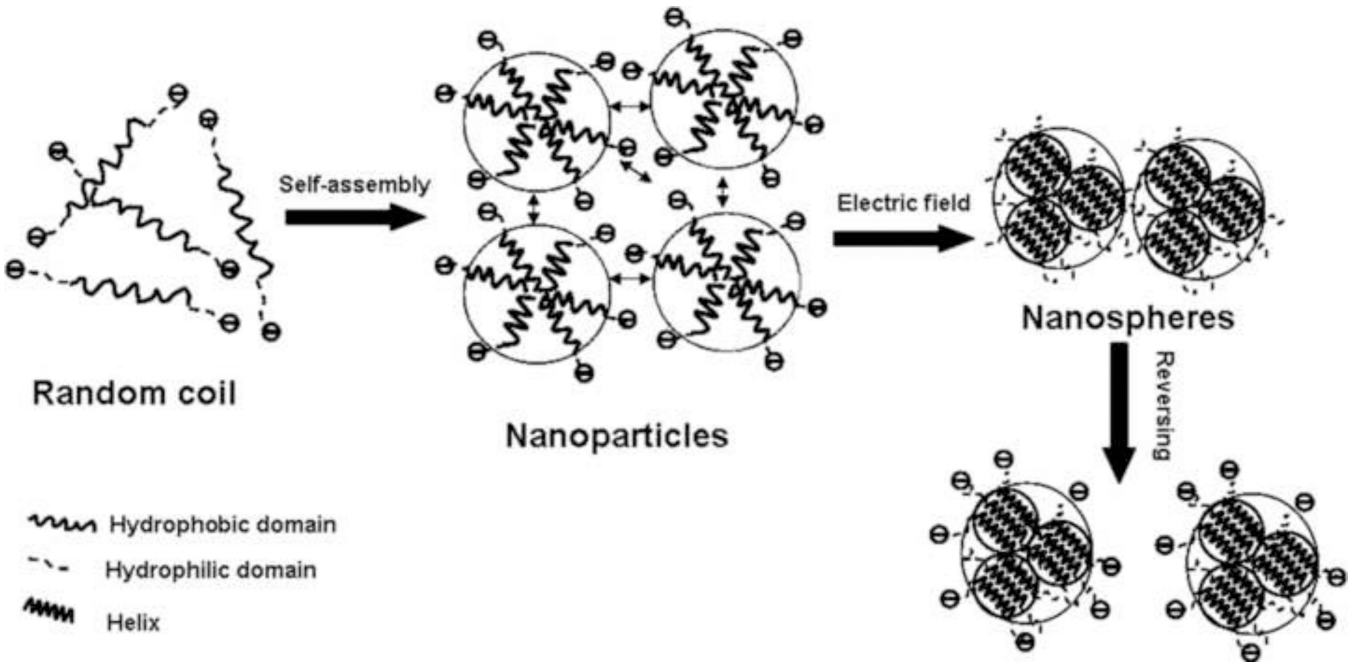

Figure 4.
Electrogelation mechanisms. Silk fibroin firstly assembled to nanoparticles with size of several ten nanometers and then further aggregated into microspheres with size up to micron. In reversing process, the microspheres dispersed into solution rather than separated into nanoparticles.

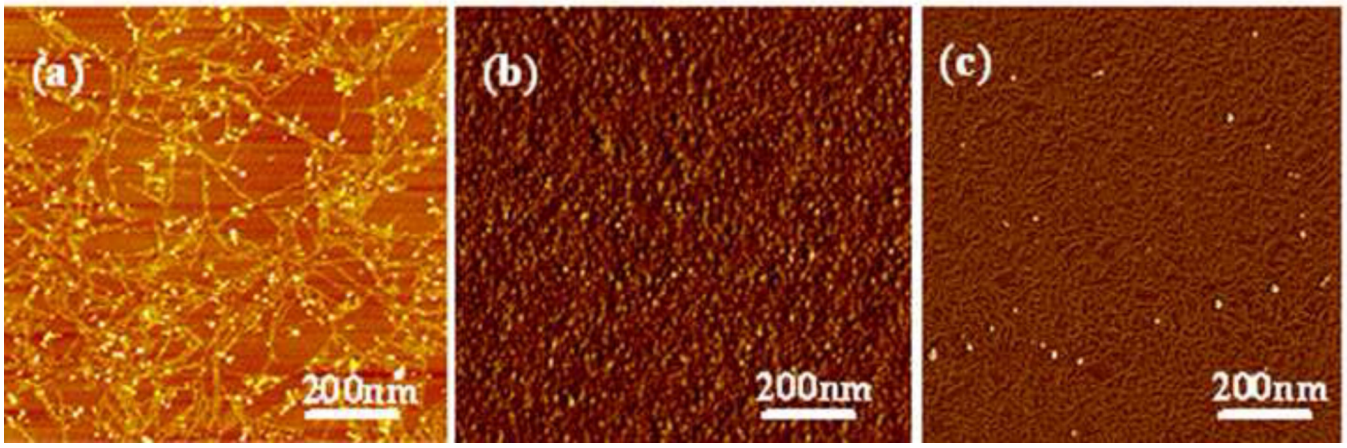

Figure 5.
AFM images of silk fibroin after different treatments: (a) fresh silk fibroin solution; (b) sample (a) incubated at 60°C for 8 hr; (c) sample (a) slowly concentrated at 60°C for 3 days. In order to avoid masking the original morphology by multilayers of silk fibroin, all samples were diluted to below 0.1 wt% before investigation.

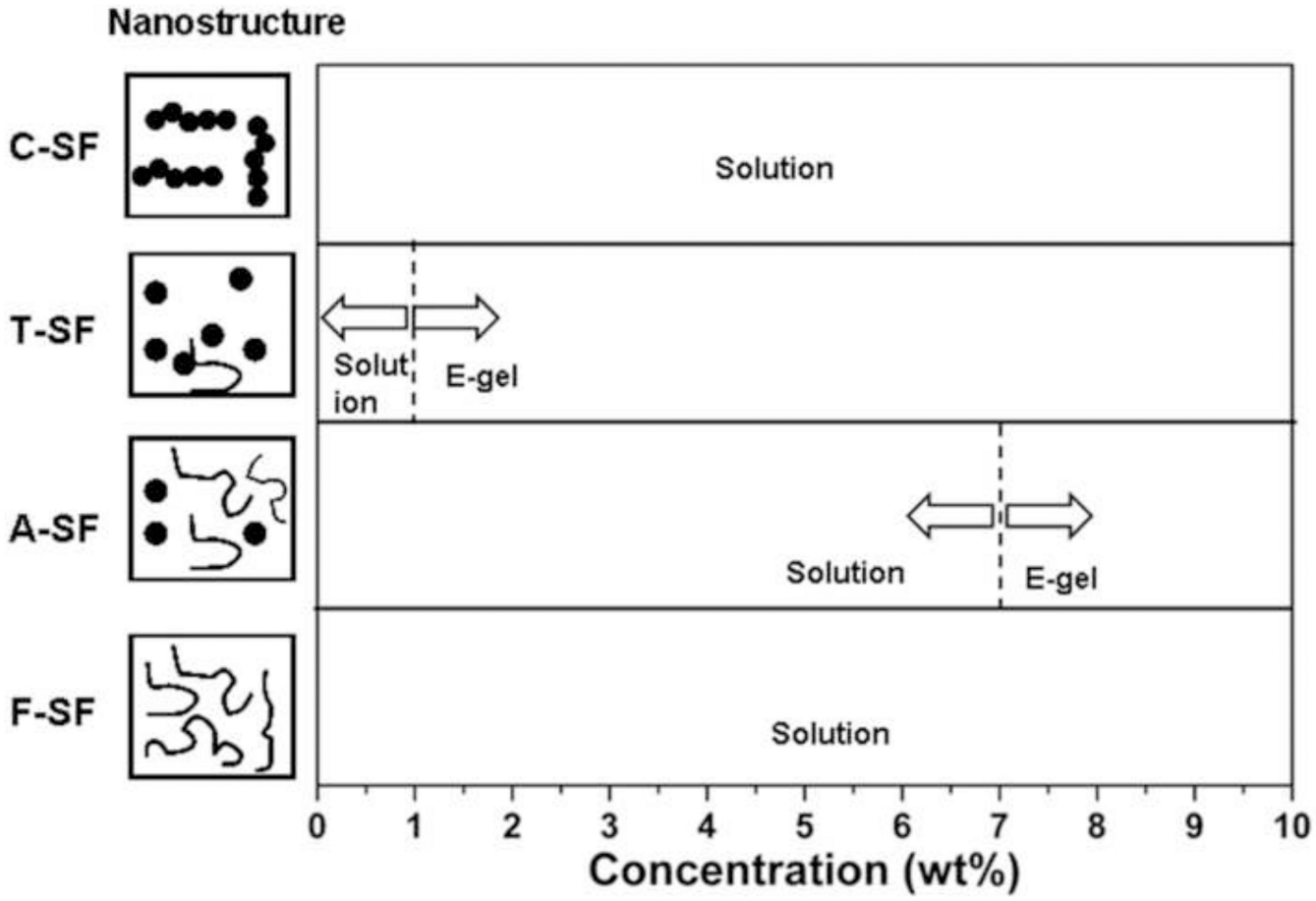

Figure 6.

E-gel formation diagram from silk fibroin solutions with different nanostructures. F-SF, fresh silk fibroin solution; A-SF, sample F-SF stored at 4°C for 2 weeks; T-SF, sample F-SF incubated 8 hr at 60°C; C-SF, sample F-SF slowly concentrated for 72 hr at 60°C. Electrogelation conditions: 25 V_{DC}, 3 min.

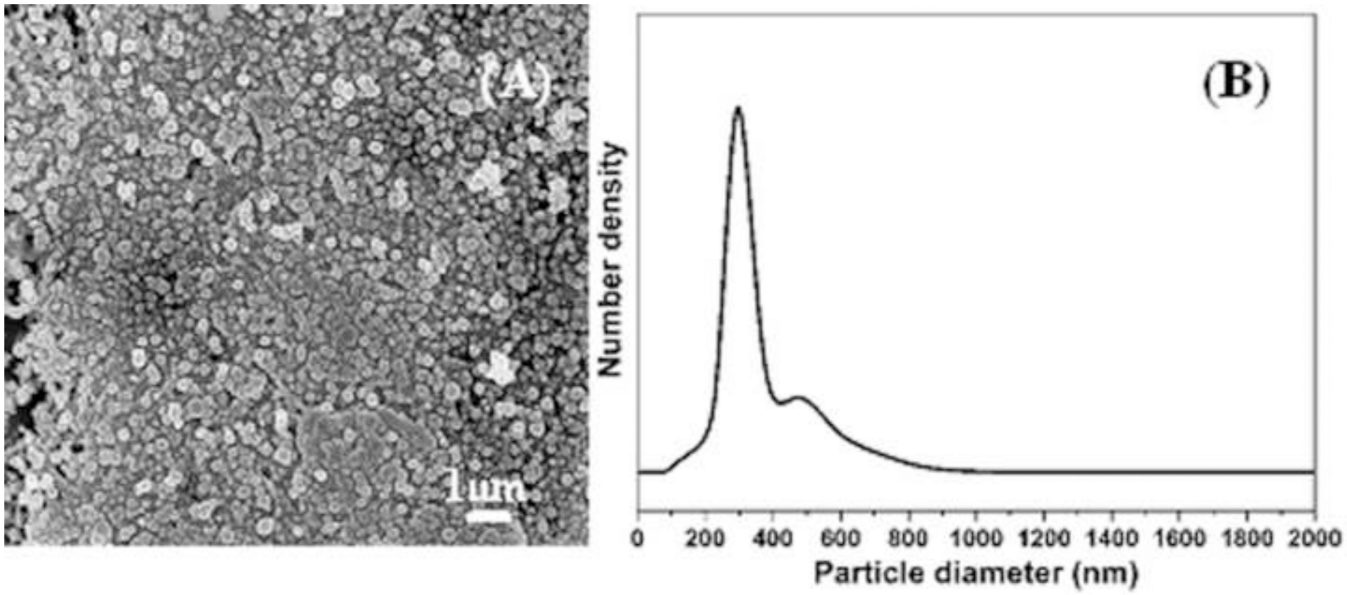

Figure 7.
A) SEM image of reversed silk fibroin solution. The sample was flash frozen and dried in liquid nitrogen. B) Size distribution of silk fibroin microspheres in the reversed solution

Table 1

The relative ratio of secondary structures in silk fibroin solutions and e-gel. F-SF, fresh silk fibroin solution; A-SF, F-SF stored 2 weeks at 4°C; E-gel, gel derived from A-SF. n=3, average±standard deviation.

Assignment	F-SF(%)	A-SF (%)	E-gel (%)
Random coil (1635–1645 cm^{-1})	26.1±2.6	18.9±2.1	15.7±1.7
Silk II, β-sheet (1610–1635 cm^{-1})	14.7±1.9	14.6±1.0	13.4±1.8
Silk I, type II β-turn (1647–1654 cm^{-1})	13.0±1.3	12.8±1.3	10.8±3.9
α-helix (1658–1664 cm^{-1})	11.0±1.5	12.5±1.1	16.2±2.0
Turns and bends (1666–1695 cm^{-1})	33.1±2.1	38.9±0.8	41.8±4.7

Table 2

E-gel formation from silk fibroin solutions with different nanostructures. F-SF, fresh silk fibroin solution; T-SF, sample F-SF incubated 8 hr at 60°C; C-SF, sample F-SF slowly concentrated for 72 hr at 60°C. All solutions were diluted to 8 wt%, 4 wt%, 2 wt% and 1 wt%, respectively. Electrogelation conditions: 25 V_{DC}, 3 min.

	F-SF				**T-SF**				**C-SF**			
Nanostructure	**Random coil**				**Nanoparticle**				**Nanofilament**			
Concentration (wt%)	8%	4%	2%	1%	8%	4%	2%	1%	8%	4%	2%	1%
E-gel formation	No	No	No	No	Yes	Yes	Yes	Yes	No	No	No	No